

Findings

of the static analysis of the arch dam Karakaya in Turkey

1. Introduction

This paper demonstrates ways of finding the optimal design of an arch dam with relatively little expenditure of time.

The arch dam is situated at the Euphrates in Turkey. The dam has a volume of 2.0 million m^3 and is 173 m in height.

This paper compares results obtained by theory of thin shells (difference method of the final design), model test, and the finite element program FLASH2.

For the sake of brevity, only the load cases self-weight and hydrostatic pressure are covered. The cases buoyancy, temperature, seismic load, shrinkage, and creep could be taken into account as well.

The program was later on extended with the following options:

- automatic input of geometry and load,
- plot possibilities for the presentation of radial and tangential deformations on the girthed shear surface,
- lines of equal concrete quality in function of a linear elastic failure criterion and spread of the concrete qualities on the building site
- consideration of seismic load according to Westergaard

The program was calibrated using long term control measurements of several older, very large arch dams.

The program POST which describes the post cooling process of fresh dam concrete is also part of the program system. It predicts temperatures on any point of the concrete, seasonal outlet temperatures in the cooling pipes, and residual stress on any point of the concrete. This thermodynamic program was calibrated using long term studies of a large gravity dam in Switzerland. This finite difference program can fulfil any arbitrary boundary conditions. With the help of this program it can be determined that a favourable horizontal compressive prestressing of the dam body of about 15 kp/cm^2 can be achieved by artificial post cooling. With this method of cooling, the seasonal mean concrete temperatures in the middle plane of the dam rise over time to the long term annual mean of the ambient air temperature. As opposed to natural cooling, with which the seasonal mean concrete temperatures in the middle plane of the dam fall over time to the long term annual mean of the ambient air temperature. Since the dam will contract using natural cooling, there is a risk of joints between certain casting segments (monoliths) partially opening.

2. Method of Calculation and Theory

The calculations were made by a computer program based on FLASH2 and its continued development. The program was used for recalculations of various existing very large arch dams. The results of the recalculations and studies of these structures were highly concordant. The finite element method was used for the static evidence. The finite element method can be defined as follows:

A method of approximation for continuum problems as follows:

- The continuum is divided into a finite number of elements whose behaviour is described by a certain number of parameters, and
- the solution of the overall system, as an accumulation of elements, strictly follows the rules applied to other standard discretisation problems.

The finite element method assumes that the mechanical behaviour of a continuously curved shell can be adequately emulated using a surface section of a polyhedron comprised of small triangles. Intuitively, it would seem that continuous refinement of the subdivision must lead to convergence. Indeed, experiments have confirmed this. This convergence has also been mathematically proven ("Arch Dams analysed by a linear finite element shell solution program"; O. C. Zienkiewicz and others).

Contrary to international concrete dam construction conventions this program uses negative signs to signify compressive stress and positive signs to signify tensile stress.

2.1 The Dam Body

To treat the double-curved shape of the Karakaya dam as a collection of flat elements, it was divided into 521 triangle-shaped finite elements in a way that angles between adjacent elements are lower than 5 degrees (10 degrees being generally acceptable). Hybrid elements were used to take shear deformations in thick shells (like Karakaya) into account. These hybrid elements are described as follows:

- There are two functions for each element. One for internal stresses and one for displaced edges.
- The assumptions for the internal stresses meet the homogeneous differential equations of the balance. However, this leads to discontinuities along the element edges (The mean is taken at the nodes).
- The functions for displaced edges of elements were chosen so that the kinematic compatibility along the edges is guaranteed.
- The matrices for stiffness, stress and load were formed in application of the principle of complementary energy so that the hybrid stress model leads to the deformation method matrix.
- All element integrations were executed numerically. This allows the use of randomly shaped triangular elements.

Results lie between the solution of a constantly too stiff behaving compatible deformation model with equivalent edge-shifting and the solution of a constantly too soft behaving pure balance model with the same stress approaches. Thus a coarse element mesh will lead to exact results as well.

2.2 Boundary Conditions

The foundation is assumed to be elastic and is simulated by an edge expansion (see Appendix Image 3). The properties of the elements (foundation elements or Vogt elements) within this expansion are determined as follows:

Based on Boussinesq's formula for an elastic half-space, Vogt calculated the shifts with regard to a norm force N , shear force Q , and momentum M distributed over a surface $b \times t$ of the plane surface of the half-space (see Fig. 1).

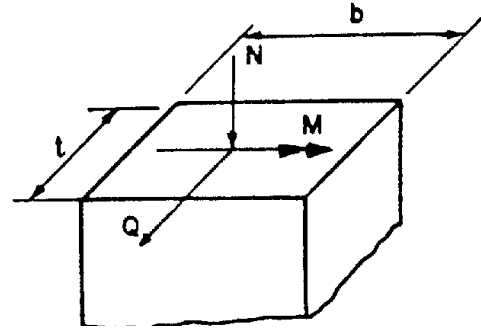


Fig. 1 Stress net force of the surface $b \times t$ on the elastic half-space

After a small change to the notations in Vogts relations between the cutting forces (N , Q , M) and the mean displacements (v_N , v_Q , v_M) gives the following:

$$\begin{bmatrix} v_N \\ v_Q \\ v_M \end{bmatrix} = \frac{1-\nu^2}{E_F} \cdot \begin{bmatrix} k & 0 & 0 \\ 0 & k & \frac{1-2\nu}{1-\nu} \cdot \frac{1}{t} \\ 0 & \frac{1-2\nu}{1-\nu} \cdot \frac{1}{t} & \frac{18}{\pi^2} \end{bmatrix} \cdot \begin{bmatrix} N \\ Q \\ M \end{bmatrix} \quad (1)$$

E_F signifies therein the modulus of elasticity of the foundation, ν Poisson's ratio, and k is a coefficient varied at the ratio of b/t (current values of k are found between 2.25 and 3.00).

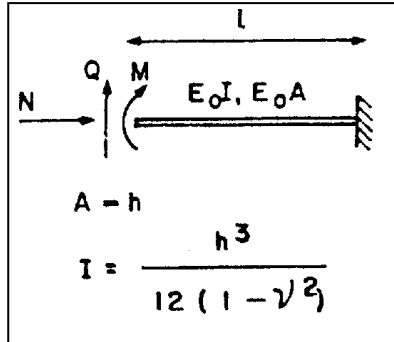


Fig. 2 Cantilever plate stressed by cutting forces

The flexibility matrix with regards to the cantilever plate in Fig. 2, which is stressed by the three cutting forces N , Q , and M and which matches the matrix (1) can be described as follows:

$$\begin{bmatrix} v_N \\ v_Q \\ v_M \end{bmatrix} = \frac{1-\nu^2}{E_0} \cdot \frac{l}{h} \cdot \begin{bmatrix} 1 & 0 & 0 \\ 0 & \frac{4l^2}{h^2} & \frac{6l}{h^2} \\ 0 & \frac{6l}{h^2} & \frac{12}{h^2} \end{bmatrix} \cdot \begin{bmatrix} N \\ Q \\ M \end{bmatrix} \quad (2)$$

Therein E_0 signifies the modulus of elasticity of the cantilever plate. There are three adjustment variables E_0 , l , and h in Matrix (2) to best match matrix (1). The component v_Q , in relation to Q can generally be neglected as emphasised by Vogt.

In all practise-oriented cases, this component is actually much smaller than the component for M . The adjustment of the central matrix element is therefor negligible. The three variables can be utilised to correct the three remaining matrix elements.

For $\nu = 0$ and $k = 2.5$ results in the following corrections:

- $h = 2.300 t$ (=115 m for Karakaya under 600 m.a.s.l.)
- $l = 0.350 t$ (=17.5 m for Karakaya under 600 m.a.s.l.)
- $E_0 = 0.061 E_F$ (=10.98 kp/cm² for Karakaya)

There is a good correlation between the displacements calculated using this method and the measurements from existing dams.

3. Assumptions with Regards to Material Properties

In accordance with the final design and the model test, the following material properties were assumed in the described calculation:

- E-Concrete = 350'000 kp/cm²
- ν -Concrete = 0.18
- E-Foundation = 180'000 kp/cm²
- ν -Foundation = 0.0 (as assumed for the Vogt elements)
- Concrete density = 2450 kg/m³

4. Dam Geometry

The element mesh was created such that the nodes lie on the shear surface of the dam (see Appendix, Image 1 and Image 2).

The thickness of each element matches the local dam stiffness in its centre of gravity.

The boundary between the dam body and the surrounding rocks was determined under usage of the final excavation plans.

Appendix, Image 3 shows an axial projection of the finite element mesh from water side. The vertical construction joints above 600 m.a.s.l. do not appear to be vertical; consequently the monoliths near the abutments appear to be smaller than those in the centre of the dam. This is due to the type of projection – and due to inconsistencies in the thickness of the dam. Appendix, Image 4 better explains this curiosity.

5. Assumptions for Dam Loads

5.1 Self-weight

The program calculates volumes of the elements automatically. Each element is self-weight loaded in its centre of gravity in negative direction to the global coordinate Z (Appendix Image 1).

For the load case self-weight, movements between neighbouring monoliths are not restricted. Thus the model representation corresponds exactly to reality. The joints between the monoliths will only be injected after self-weights have fully taken effect.

5.2 Hydrostatic Pressure

The hydrostatic load is assumed to affect each element uniformly spread. This load is equal to the product of

- the hydrostatic pressure at centre of gravity of the element for a water level of 693 m.a.s.l., and
- the projection area of the element on the water-side surface of the dam wall (due to the curvature of the dam, the surface which is impacted by the water load is larger than that of the element mesh).

Due to the slopes of the centre surface between elevations of 610,37 and 678,69 m.a.s.l. (Appendix Image 2) the resulting hydrostatic forces were split into two; one parallel and the other normal to the concerned element surface.

cm²

6. Conclusions

6.1 Stresses

The symbols in Appendix, Image 5 and Image 6 show direction and size of the main stresses for the load combination of self-weight and hydrostatic pressure on the water and air side respectively. The stresses are generally below 45 kp/cm² for the pressure areas and 20 kp/cm² for the tensile areas. This is not the case for the edges of the spillway where limited stress concentrations will develop due to notch effects according to Neuber. There, the maximum compressive stresses can reach a theoretic value of 75 kp/cm².

The dam outline exhibits an unusual form. This is due to the spillway being inserted into the dam wall. Statically speaking, the structure does not have an optimal shape. This is evident in the stress distribution. In particular in the central areas of the air side surface of the dam, where tensile stresses for the combination self-weight and hydrostatic pressure prevail.

6.2 Displacements

Appendix, Image 7 shows lines of equal displacements in the global direction X (Appendix Image 1) for the load case of hydrostatic stress. The load case of self-weight was excluded, because control measurements can only be made after the construction is completed.

One can observe that the dam crest is slightly raised as a result of the hydrostatic stress. This phenomenon can be explained with Poisson's lateral strain, which is caused by horizontal compressive stress from the arching effect.

Appendix, Image 8 shows the shapes of the original and the deformed element meshes. The magnification factor is 1000. This image does not provide quantitative insight, but it helps to better understand the global behaviour of an arch dam.

7. Comparison of the Conclusions with those of the Difference Method and Model Test

Appendix, Images 9 through 13 are selected graphs comparing the stresses and displacements determined via the finite element method, the difference method (final design), and the model test. Of particular importance is the observation that results of the finite element calculation generally lies between those of the other two methods. The model test provides the largest values for stresses and displacements. The displacements were split into radial and tangential directions to allow comparisons with earlier analyses.

The graphs in Appendix Image 9 show the 'vertical' stresses in the centre of spillway for hydrostatic loads only. Due to the predominant shell action in this zone, compressive stresses

prevail on the water side surface of the dam whereas tensile stresses prevail on the air side of the dam. On the basis of the model tests, it seems that the results of the finite element analysis are closer to reality than those of the difference method (final design).

The graph shows comparatively high tensile stresses on the water side surface below 550 m.a.s.l. The resulting tensile stresses of superimposition of the load cases self-weight and hydrostatic pressure however never exceed a value 18 kp/cm^2 .

Appendix, Image 10 shows the graph of the horizontal stresses in the centre of the spillway. The graph shows that the horizontal stresses reduce with decreasing elevation. From this it can be derived that the arching effect prevails in the upper sections whereas console force prevails in the lower sections.

Appendix, Image 11 shows the horizontal stresses at elevation of 675 m.a.s.l. The significant discontinuities at about 90 m left and right of the dam centre are noteworthy. This irregularity relates to the stress concentration at points with significant changes to the outline of the dam at the sides of the spillway.

Appendix, Images 12 and 13 show the graphs of the radial and tangential displacements of the shear surface of the dam in the centre of the spillway and at elevation of 675 m.a.s.l.

The radial displacements as calculated using the finite element method are slightly larger than those calculated using the difference method (final design). This is directly linked to the fact that shear deformations are neglected using the difference method (theory of thin shells).

Whereas the finite element method includes these additional deformations (hybrid expression).

It can be observed, that the radial displacements measured on the model are significantly larger than those calculated. This phenomenon can be related to the following assumptions for the analytical methods:

- The dam is based on the plane surface of the elastic half-space (Vogt elements).
- The elastic moduli of the dam body as well as those of the rock abutments were assumed to be constant during loading and unloading (that is the dam concrete and the surrounding rock possess an ideal elasticity; there is no hysteresis).

In reality, these theoretical assumptions present additional links, which cannot be reproduced on the model. Which means that the model will always produce larger deformations.

8. Conclusions

A priori the following can be determined:

- The results of the above finite element analysis can be confirmed using the results of earlier finite difference calculations (final design) and model tests.
- The fracture pattern at the end of the model test confirms the prediction of place, direction, and magnitude of the main tensile stresses on the lower air side of the dam.
- Using the Karakaya arch dam as an example, it can be observed that the idea of an arch gravity dam does not apply. Such a wall behaves as a normal shell (that is, the normals on the shear surface stay normal before and after deformation).
- Much more refined results can be obtained through the usage of hybrid plate-shell-elements instead of solid elements.
- The program is able to find the optimal shape of an arch dam in a short time.

Zürich, 13th May 2015
Rudolf Trinkner, Dr. sc. techn. ETH
Maneggpromenade 82
CH-8041 Zürich
044 9844987

Appendix

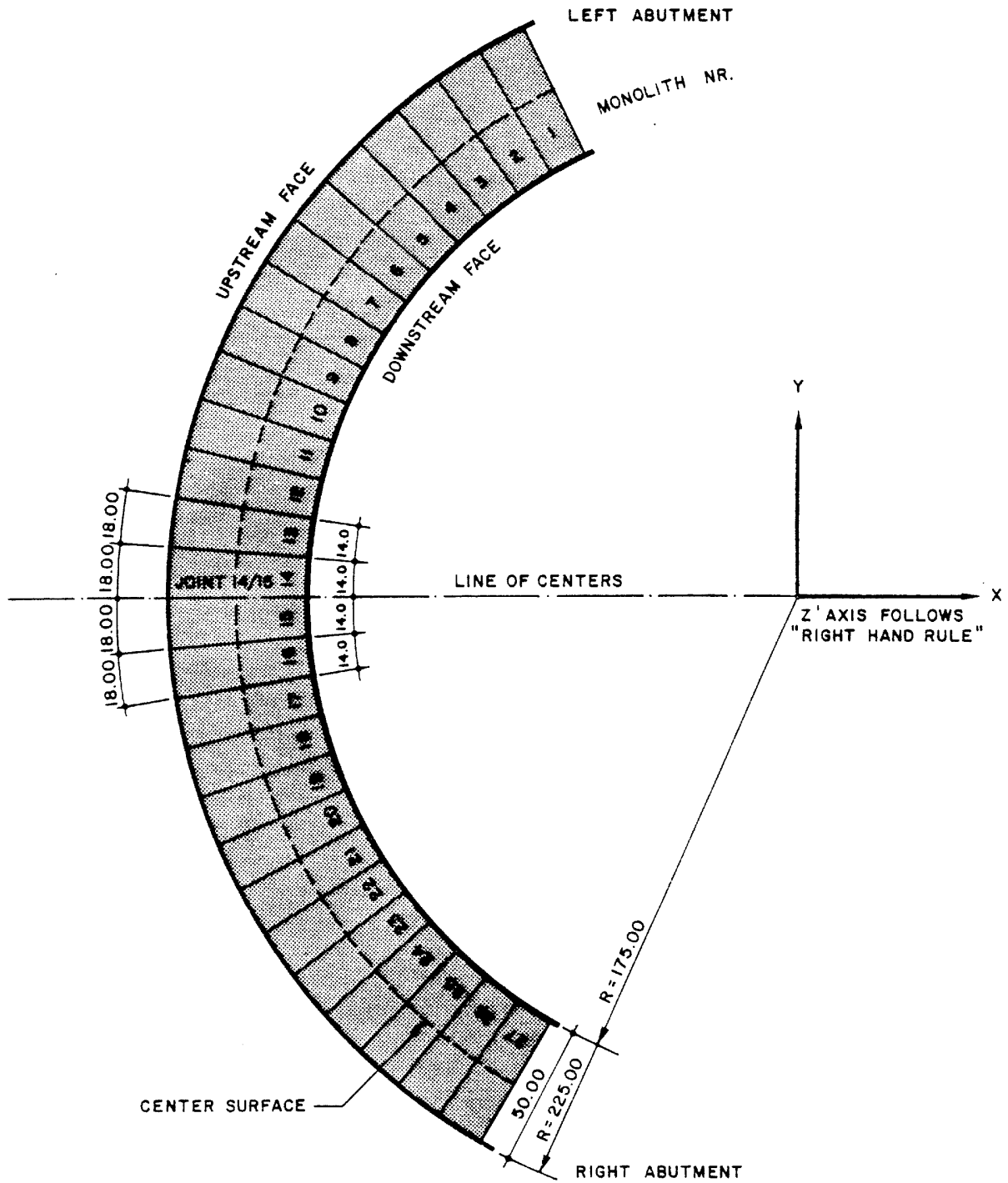


Image 1

Dam geometry and coordinate system for the definition of load directions in the outline

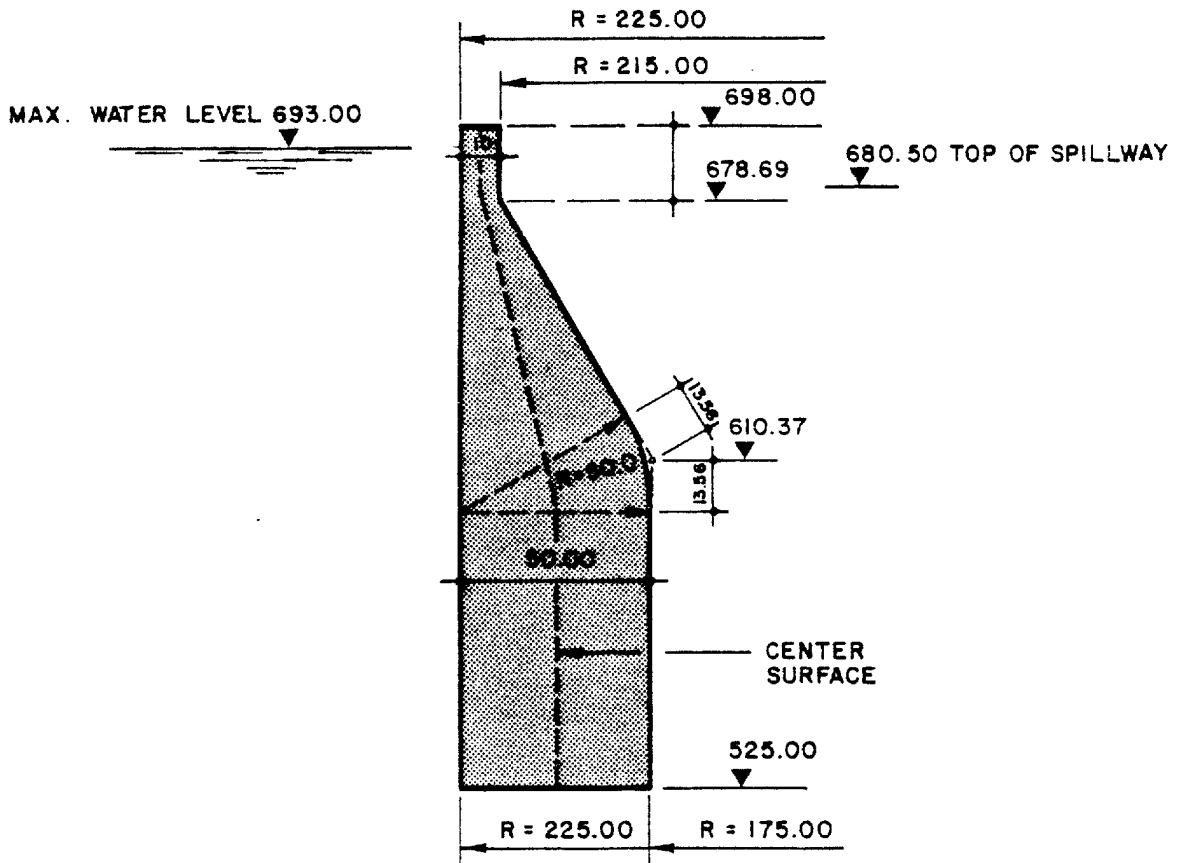


Image 2

Typical cross section of a dam

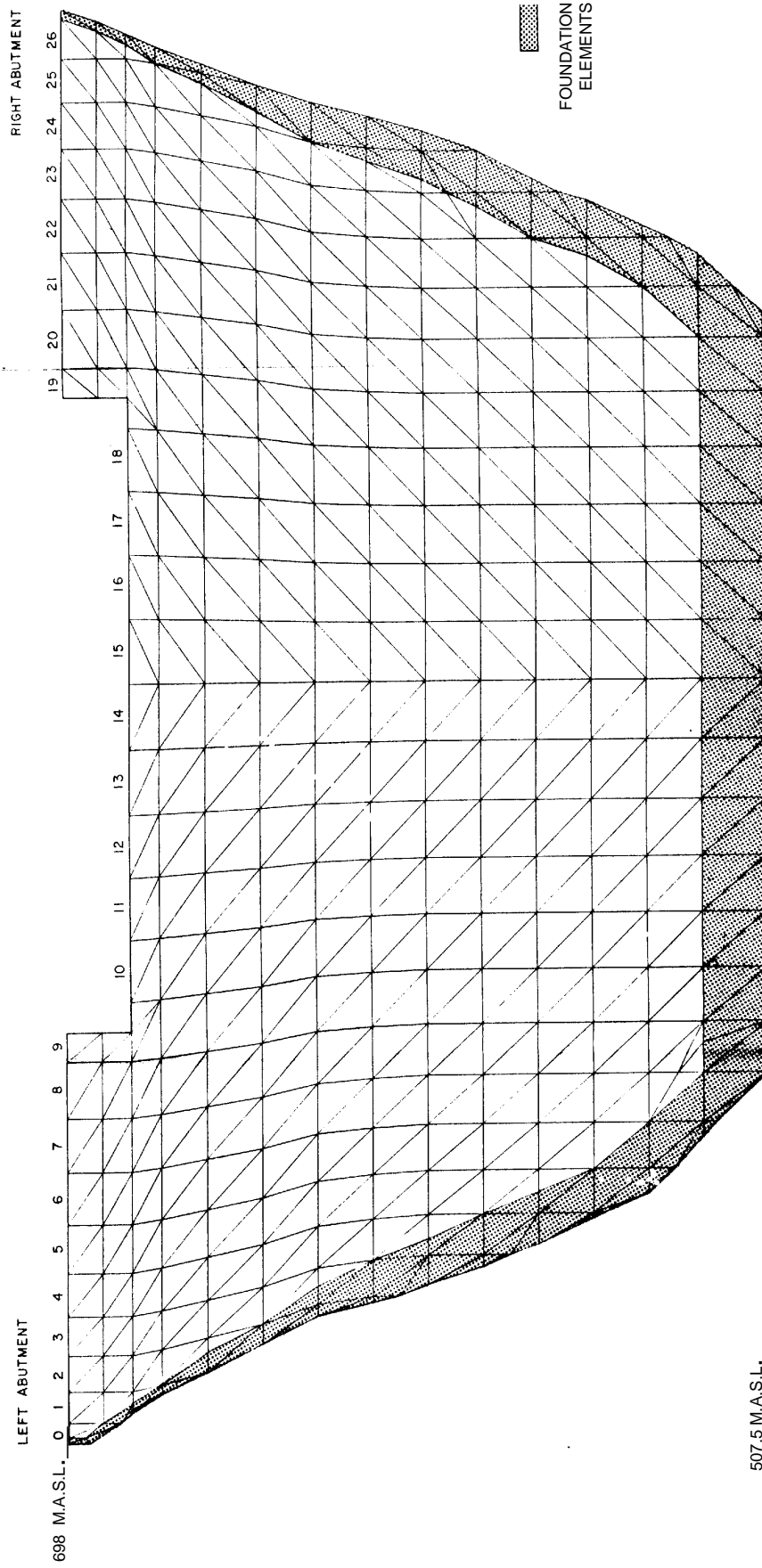


Image 3

Water side view of the element mesh

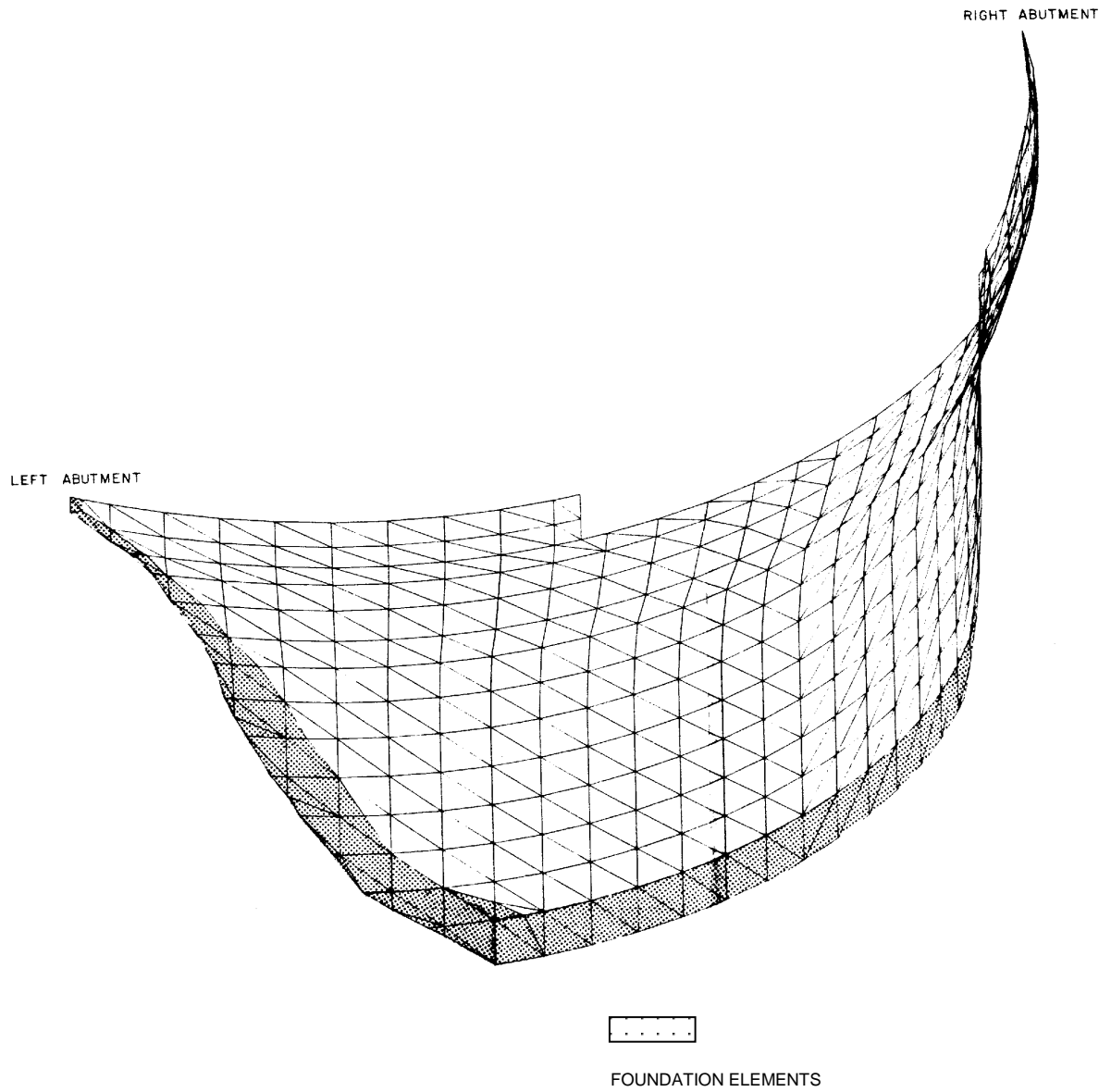


Image 4
Spatial view of the element mesh

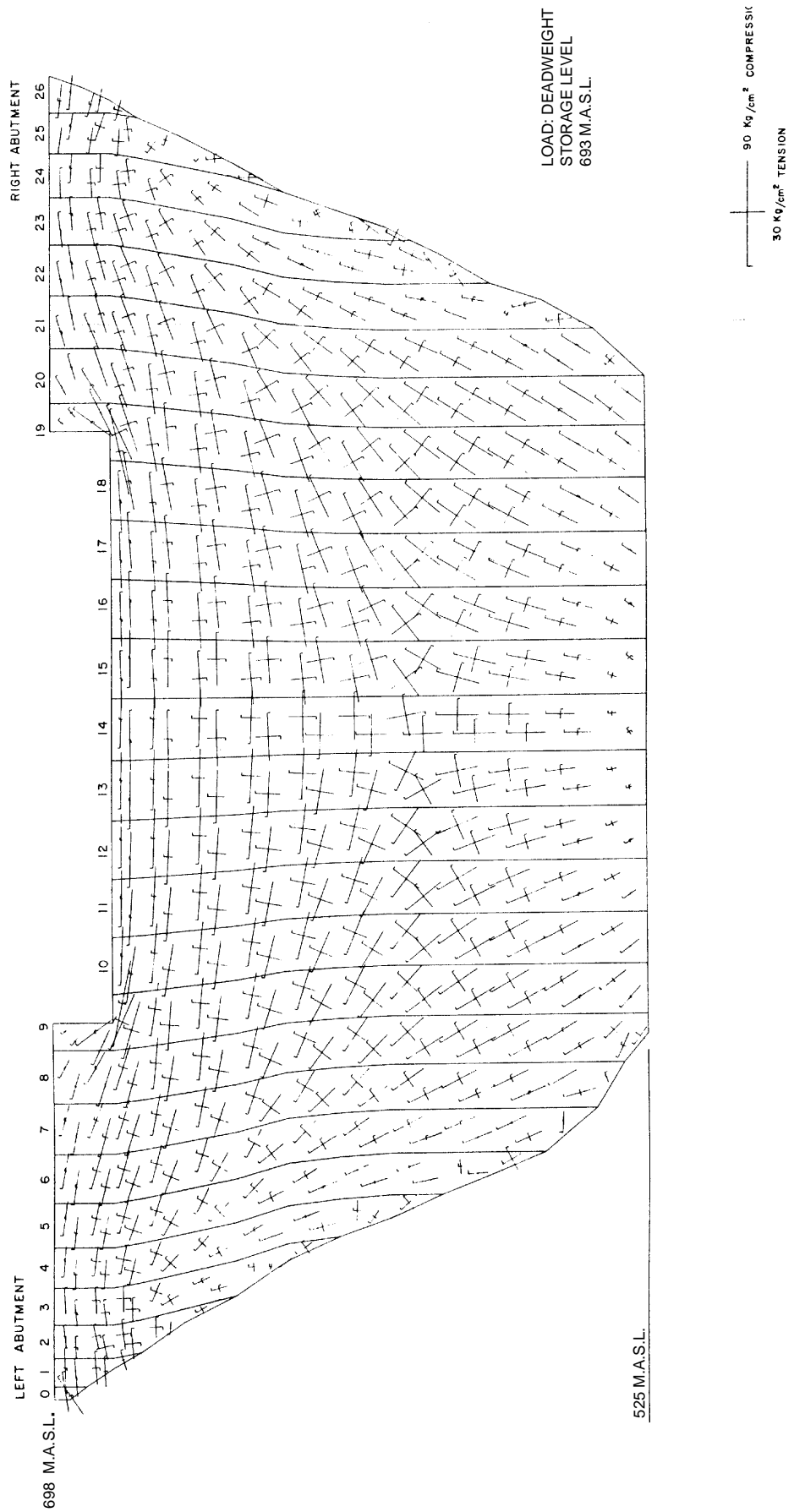


Image 5

Main stresses on the water side surface of the dam

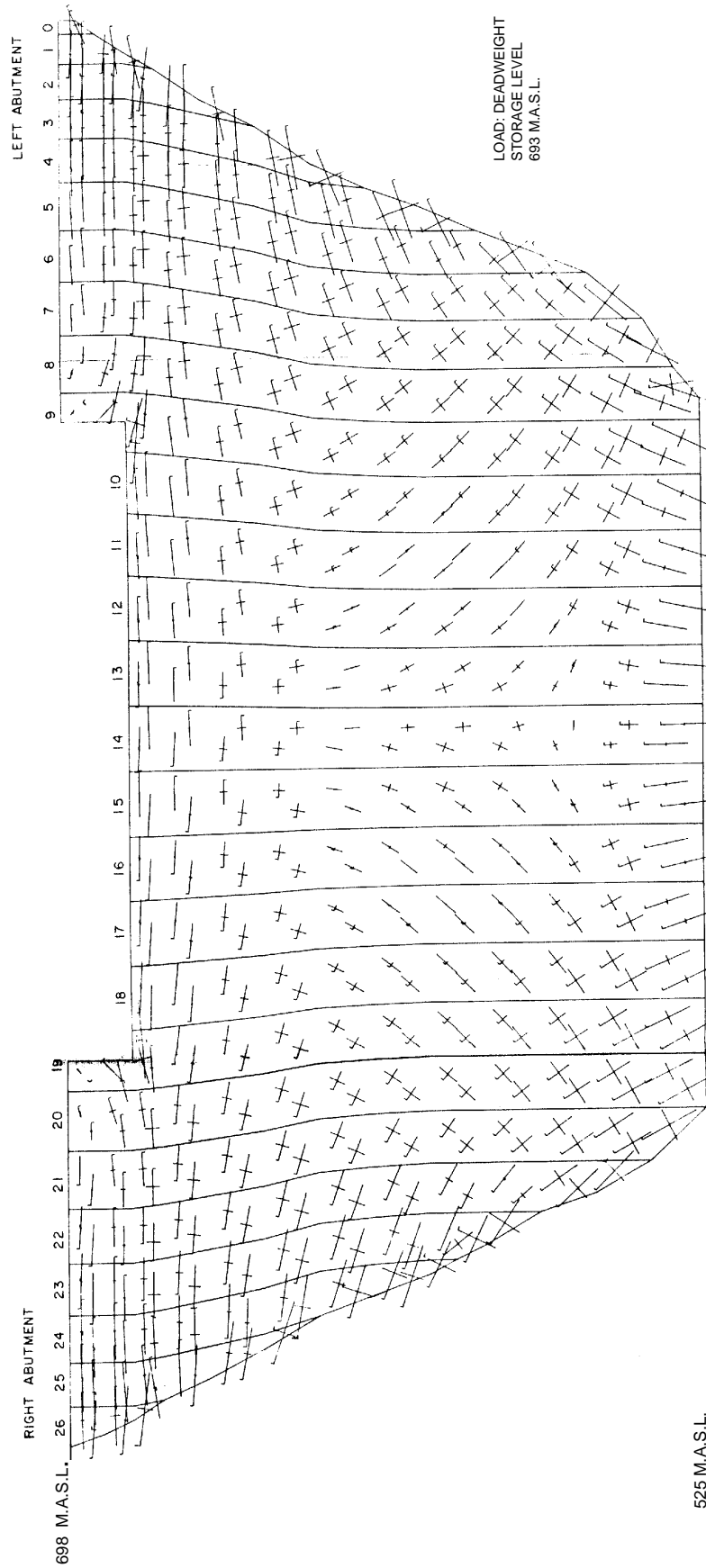


Image 6
Main stresses on the air side surface of the dam

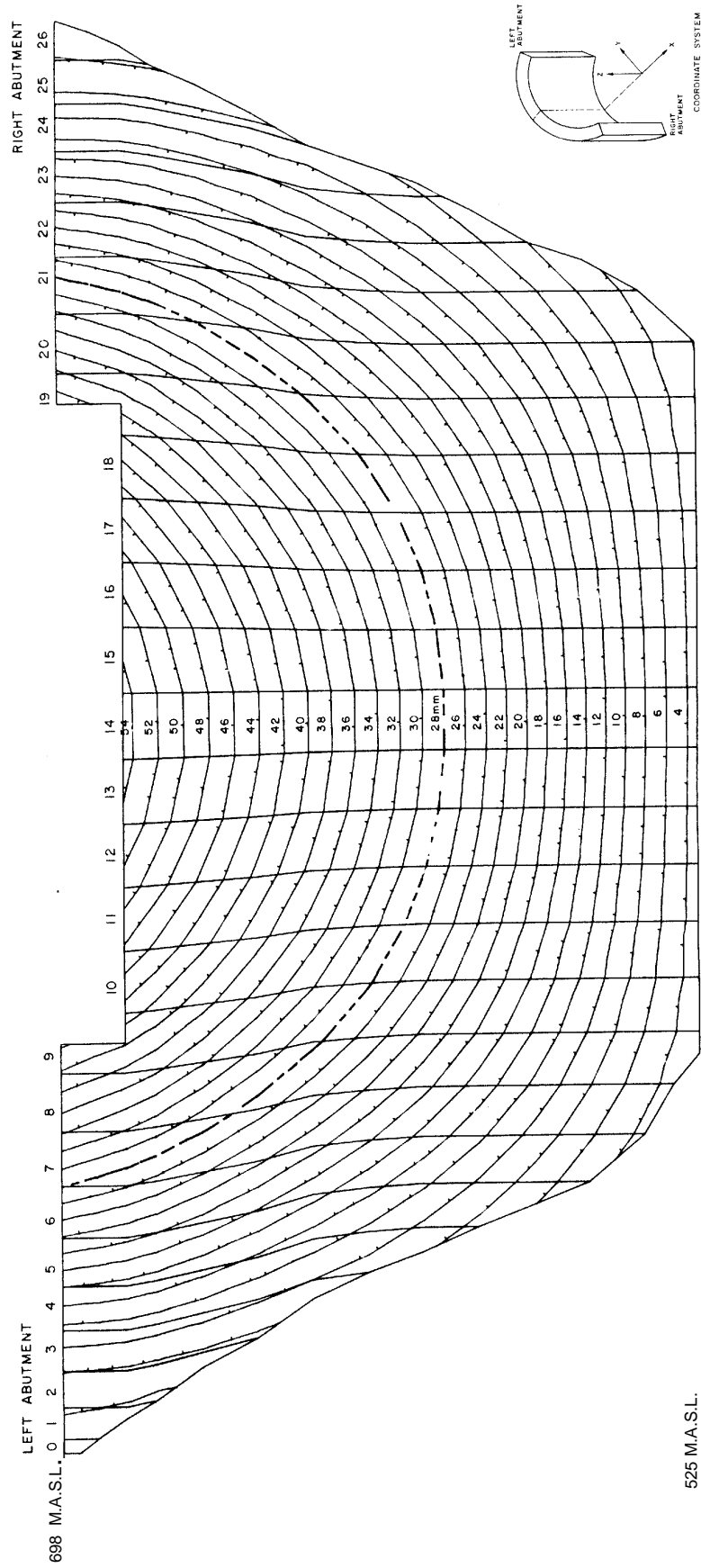


Image 7
 Displacements in the direction of the X (mm)

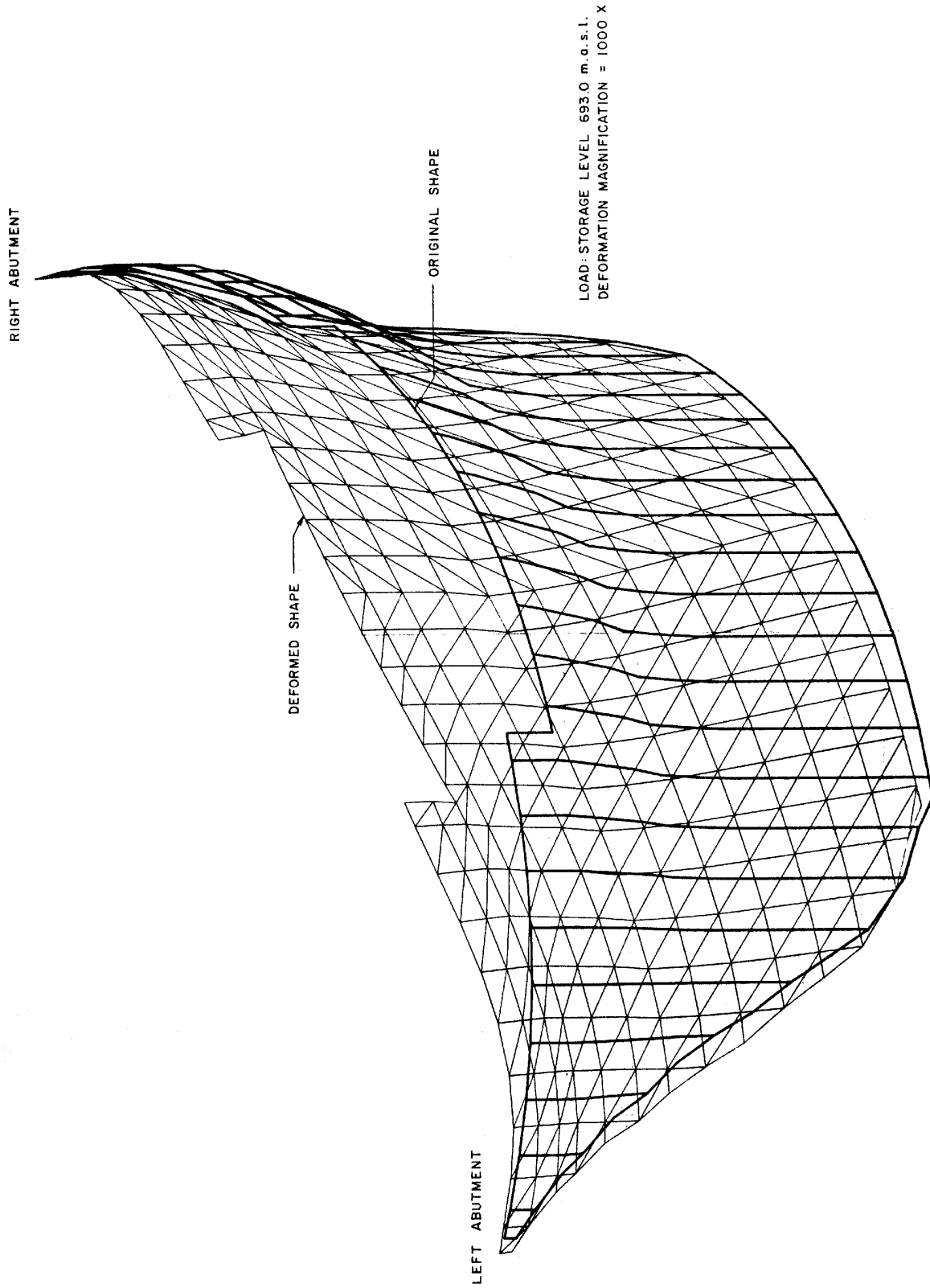


Image 8

Spatial view of the deformed element mesh

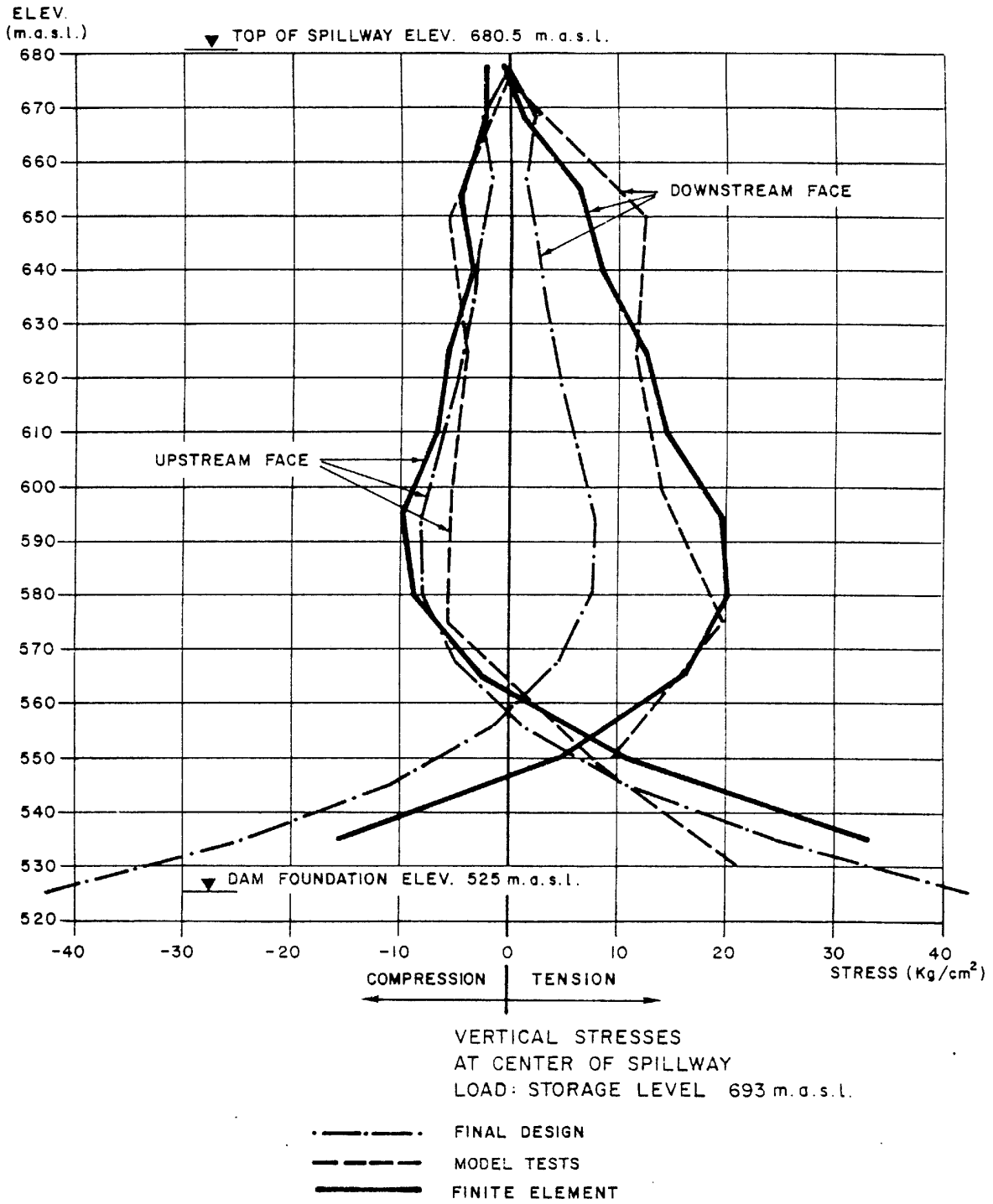


Image 9

Vertical stresses at the centre of the spillway due to hydrostatic load

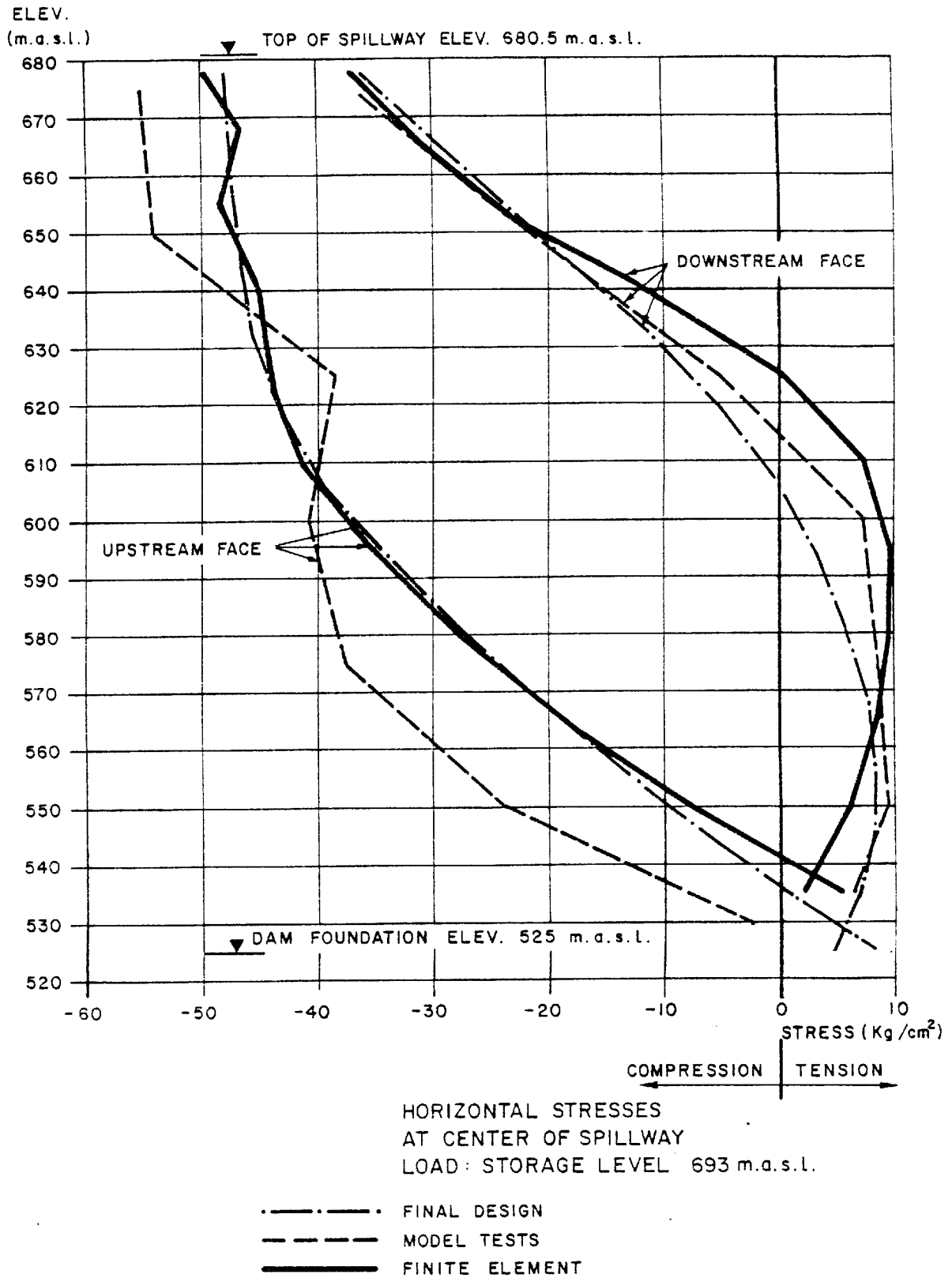


Image 10

Horizontal stresses at the centre of the spillway due to hydrostatic load

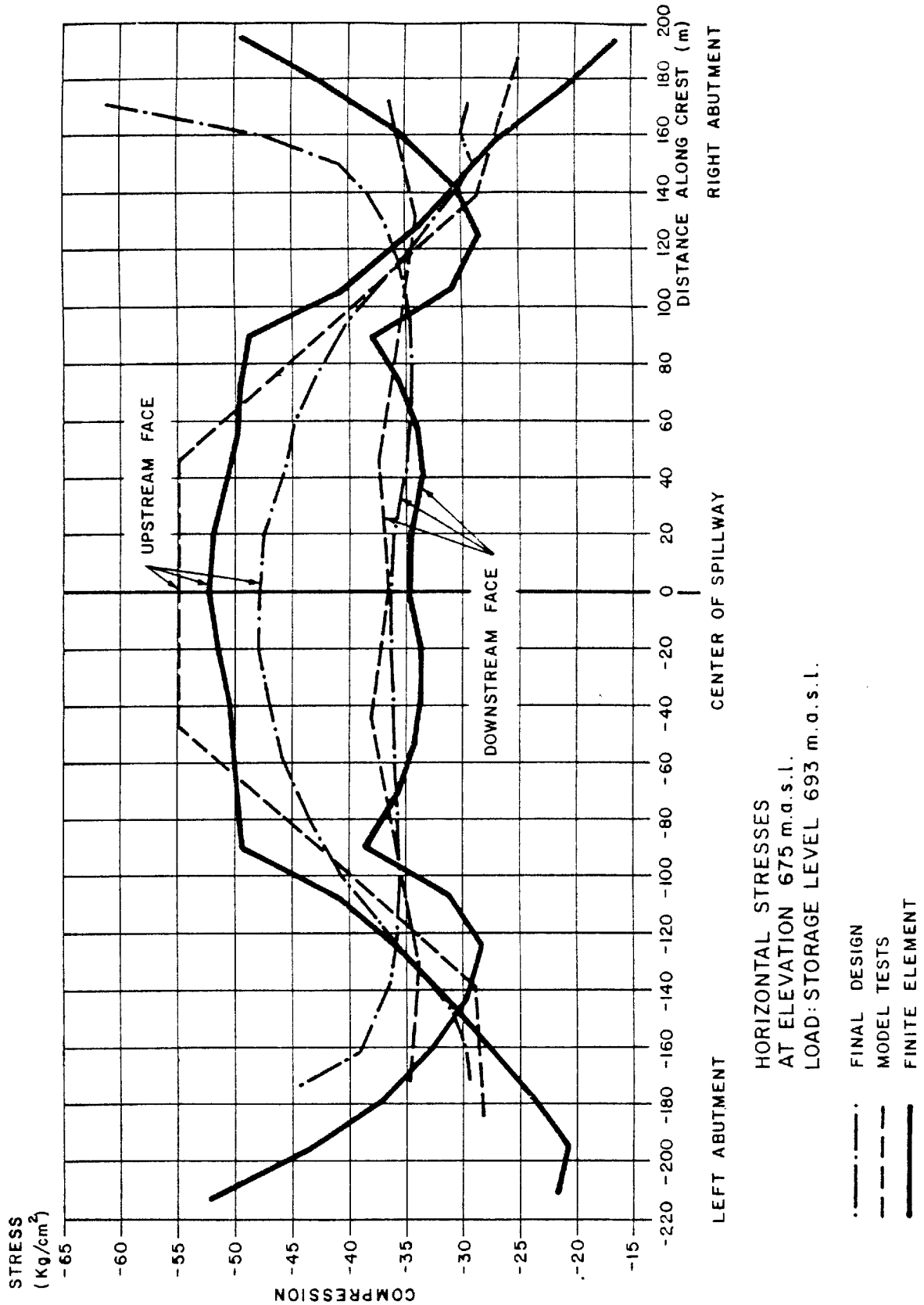
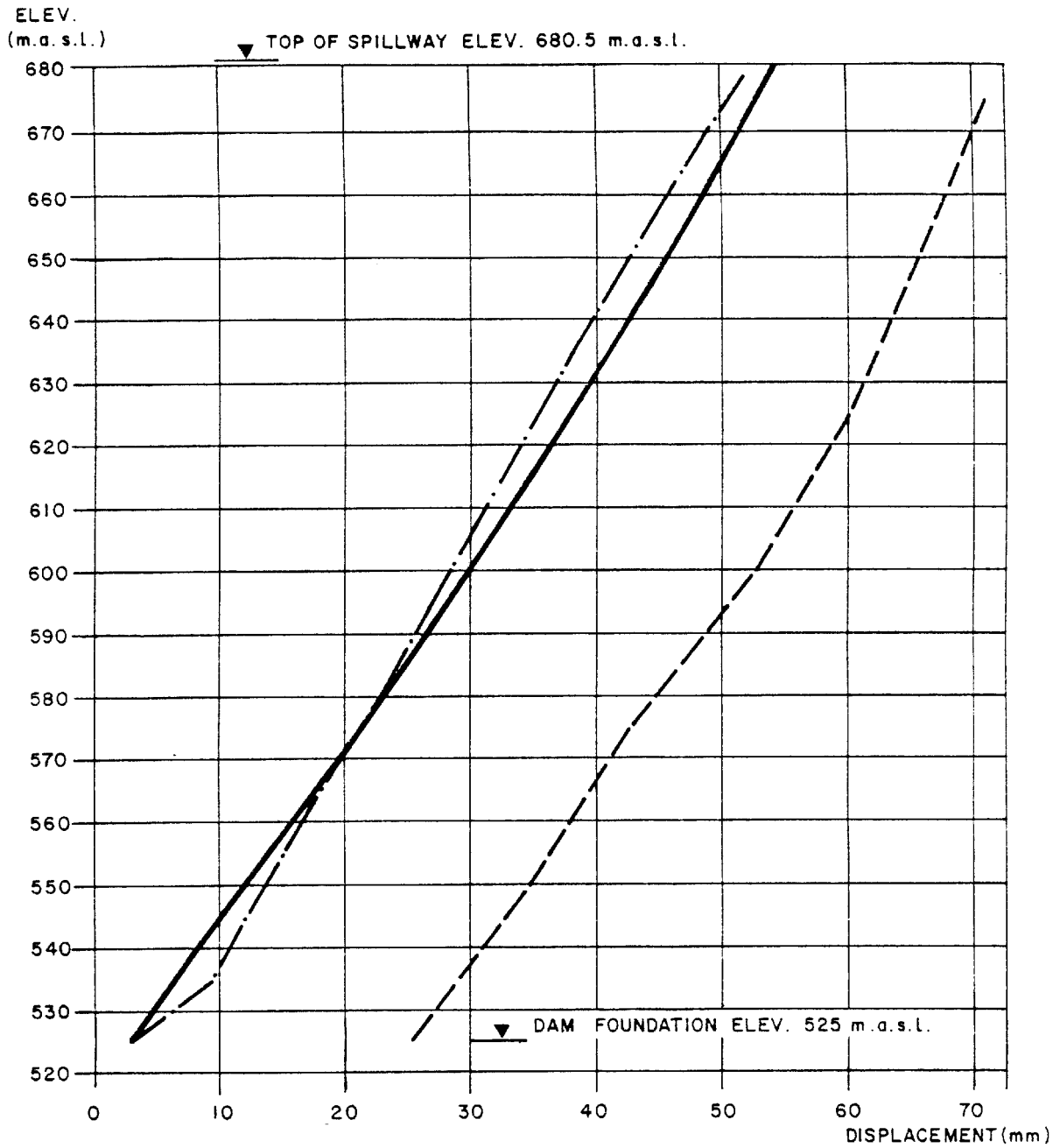


Image 11

Horizontal stresses at elevation of 675 m.a.s.l. due to hydrostatic load



HORIZONTAL RADIAL DISPLACEMENTS
 AT CENTER OF SPILLWAY
 LOAD: STORAGE LEVEL 693 m.a.s.l.

- - - - - - FINAL DESIGN
- - - - - MODEL TESTS
- FINITE ELEMENT

Image 12

Horizontal radial displacements at the centre of the spillway due to hydrostatic load

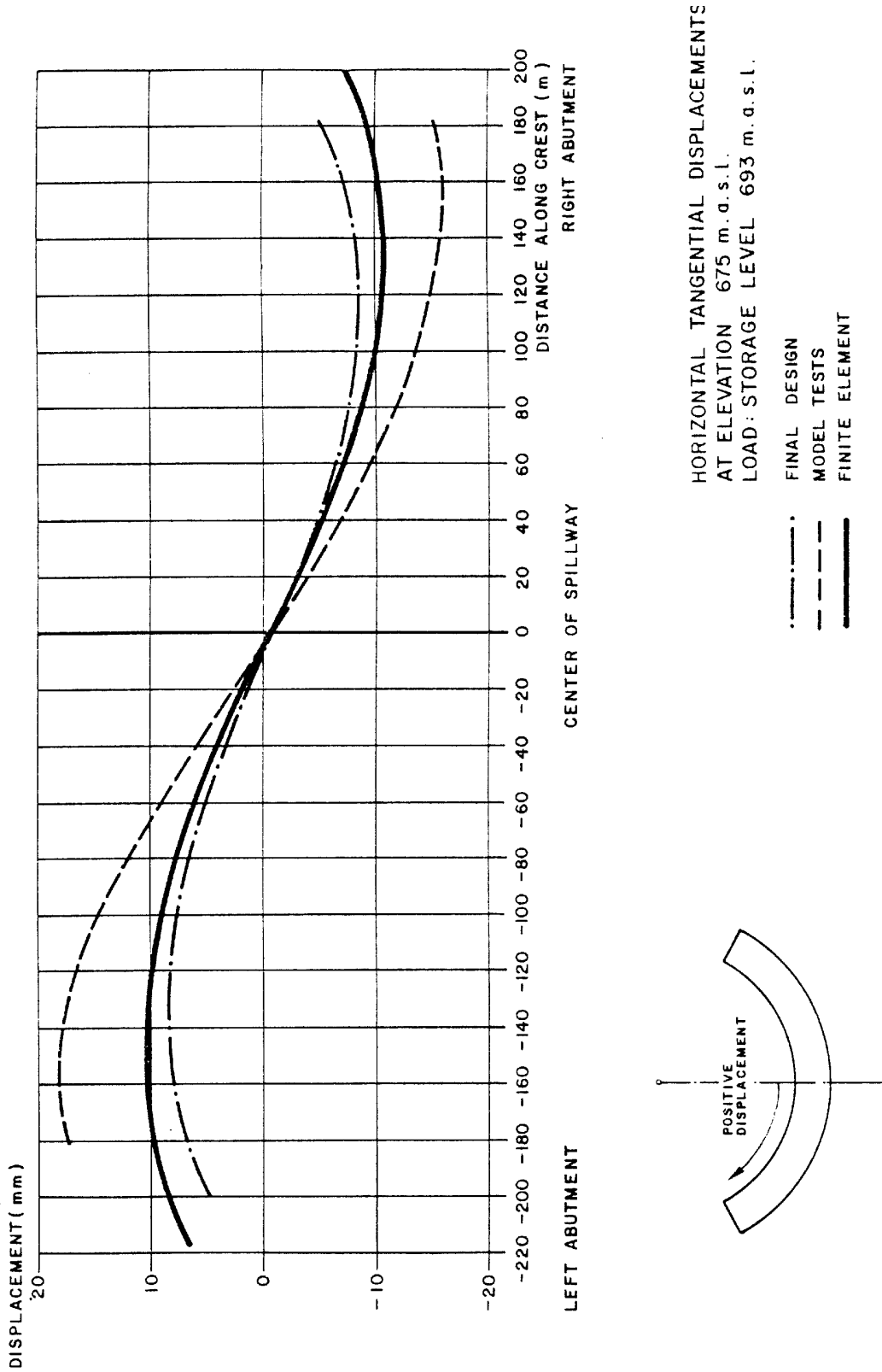


Image 13

Horizontal tangential displacements of the dam at elevation of 675 m.a.s.l. due to hydrostatic load